TISSUE ENGINEERING: Part A
Volume 21, Numbers 3 and 4, 2015

DOI: 10.1089/ten.tea.2014.0177

Functionalization of Polycaprolactone Scaffolds with Hyaluronic Acid and β-TCP Facilitates Migration and Osteogenic Differentiation of Human Dental Pulp Stem Cells *In Vitro*

Jonas Jensen, MD,[1,2] David Christian Evar Kraft, MSc, PhD,[3] Helle Lysdahl, MSc, PhD,[1] Casper Bindzus Foldager, MD, PhD,[1] Muwan Chen, MSc, PhD,[1,4] Asger Albæk Kristiansen, MSc,[4] Jan Hendrik Duedal Rölfing, MD, PhD,[1,5] and Cody Eric Bünger, MD, DMSc[1,5]

In this study, we sought to assess the osteogenic potential of human dental pulp stem cells (DPSCs) on three different polycaprolactone (PCL) scaffolds. The backbone structure of the scaffolds was manufactured by fused deposition modeling (PCL scaffold). The composition and morphology was functionalized in two of the scaffolds. The first underwent thermal induced phase separation of PCL infused into the pores of the PCL scaffold. This procedure resulted in a highly variable micro- and nanostructured porous (NSP), interconnected, and isotropic tubular morphology (NSP-PCL scaffold). The second scaffold type was functionalized by dip-coating the PCL scaffold with a mixture of hyaluronic acid and β-TCP (HT-PCL scaffold). The scaffolds were cylindrical and measured 5 mm in height and 10 mm in diameter. They were seeded with 1×10^6 human DPSCs, a cell type known to express bone-related markers, differentiate into osteoblasts-like cells, and to produce a mineralized bone-like extracellular matrix. DPSCs were phenotypically characterized by flow cytometry for $CD90^+$, $CD73^+$, $CD105^+$, and $CD14^-$. DNA, ALP, and Ca^{2+} assays and real-time quantitative polymerase chain reaction for genes involved in osteogenic differentiation were analyzed on day 1, 7, 14, and 21. Cell viability and distribution were assessed on day 1, 7, 14, and 21 by fluorescent-, scanning electron-, and confocal microscopy. The results revealed that the DPSCs expressed relevant gene expression consistent with osteogenic differentiation. The NSP-PCL and HT-PCL scaffolds promoted osteogenic differentiation and Ca^{2+} deposition after 21 days of cultivation. Different gene expressions associated with mature osteoblasts were upregulated in these two scaffold types, suggesting that the methods in which the scaffolds promote osteogenic differentiation, depends on functionalization approaches. However, only the HT-PCL scaffold was also able to support cell proliferation and cell migration resulting in even cell dispersion throughout the scaffold. In conclusion, DPSCs could be a possible alternate cell source for bone tissue engineering. The HT-PCL scaffold showed promising results in terms of promoting cell migration and osteogenic differentiation, which warrants future *in vivo* studies.

Introduction

Scaffolds for bone tissue engineering have undergone rapid development through the past two decades, mainly due to an increased understanding of the underlying mechanical, chemical, and biological mechanisms necessary to achieve enhanced bone regeneration.[1,2] One primary goal in scaffold construction for bone regeneration, is to manipulate the micro- and nanoscale characteristics of the scaffold. This is done in order to stimulate cell migration and osteogenic differentiation, while achieving biocompatibility and dissuading a foreign body response.[3,4]

Microscale manipulation is known to be able to alter cell migration and nutrient flow, whereas alterations in the nanoscale topography plays a key role in the induction of stem cell differentiation and osteogenesis.[5] Fused deposition modeling (FDM) has been developed as a promising method for macro- and micro-structuring in polycaprolactone (PCL)

[1]Orthopaedic Research Laboratory, Aarhus University Hospital, Aarhus, Denmark.
[2]Department of Radiology, Aarhus University Hospital, Aarhus, Denmark.
[3]Department of Orthodontics, School of Dentistry, Aarhus University, Aarhus, Denmark.
[4]Interdisciplinary Nanoscience Center (iNANO), Aarhus University, Aarhus, Denmark.
[5]Department of Orthopaedics, Aarhus University Hospital, Aarhus, Denmark.

scaffold manufacturing.[6,7] Utilizing FDM, each scaffold can be custom-made to accommodate challenges of different bone void dimensions without losing the desirable feature of scalable and cost-effective industrial production.[8] One drawback of current technologies in FDM manufacturing is the lack of capabilities to control nanoscale topography. One way to overcome this challenge is by modifying parts of the scaffold by utilizing thermal induced phase separation (TIPS), a process that results in a highly porous scaffold with isotropic tubular morphology and extensive pore connectivity. Combined control of macroscopic dimensions of the backbone structure and the micro- and nano-porous morphology can be achieved by combining these two manufacturing methods.[9,10] Another way to functionalize the FDM-manufactured PCL scaffolds is by coating the polymer surface with other bioactive compounds such as hyaluronic acid (HA). HA is a naturally occurring nonimmunogenic glycosaminoglycan and plays a significant role as a facilitator of osteogenic differentiation and as a migration-stimulating agent for mesenchymal stem cells (MSCs).[11,12] The hydrophilic properties of HA can furthermore be utilized to decrease the inherent hydrophobic property of PCL. To further enhance the osteoconductive properties, β-tricalcium phosphate (β-TCP) can be added to the coating solution. This HA/β-TCP coating does not aim to provide additional mechanical strength to the scaffold and, because of the degradation time of HA, will be degraded within the first 3 weeks. The coating was intended to provide the above stated potentially beneficiary properties to the scaffold during the first weeks of cell migration, proliferation, and osteogenic differentiation. This surface coating has recently shown favorable osteogenic properties both *in vitro* and in a subcutaneous mouse study.[13]

Another approach to functionalize the scaffolds prior to implantation is to seed them with autologous MSCs. Bone marrow-derived MSCs (BMSCs) have traditionally been the multipotent cell of choice in bone tissue engineering because of their ability to differentiate into osteoblasts and stimulating the bone-healing environment by recruiting stem cells and osteoblasts from the adjacent tissue.[14,15] BMSCs exhibit a short population doubling (PD) range of approximately 30 before cell senescence, and loss of phenotypic behavior (osteodifferentiation and bone forming capacity) upon culturing. This limits expansion potential *in vitro* and cause concern regarding reproducibility of *in vitro* experiments where BMSCs are used.[16] Furthermore, only one out of every ten thousand cells in the bone marrow express MSC characteristics, thus limiting the cell pool available from a biopsy.[17] Additional sources of osteogenic multipotent cells are therefore currently being explored.[4] Dental tissues are considered an alternative source for harvesting MSC-like populations.[18] Ecto-mesenchymal dental pulp-derived stem cells (DPSCs) originating from the dentin/pulp complex represent a cell line with a high and stable yield upon harvest.[19,20] DPSCs are known to express bone-related markers similar to BMSCs and the ability to produce more colony forming units, exhibit more PDs before cell senescence, and elicit higher proliferation rates than BMSCs.[21,22] DPSCs have displayed the ability to differentiate into osteoblasts-like cells and produce a bone-like mineralized extracellular matrix (ECM) and a bone-like trabecular structure.[23–25] Consequently, cell cultures originating from the dental pulp have received increased attention for application in bone tissue engineering.[18,26,27]

Our main hypothesis was that functionalizing FDM-manufactured PCL scaffolds with either a TIPS-manufactured PCL compound or a HA/β-TCP coating, would increase the osteogenic differentiation of DPSCs and mineralization (Ca^{2+} deposition) on the scaffold.

Thus, the main aim of this study was to compare the osteogenic differentiation of human DPSCs when seeded on three FDM-manufactured scaffolds with different structural compositions and functionalizations.

Materials and Methods

Scaffold manufacturing

Rapid prototyping by FDM was utilized to fabricate the three-dimensional (3D) mesh compound of the scaffolds. PCL polymer with a molecular weight of 50 kDa (Perstorp UK, Cheshire, United Kingdom) was used. The scaffolds were built from layered deposition of PCL strands as previously described.[10] To increase surface hydrophilicity, the scaffolds were treated with 5 M NaOH for 3 h, neutralized with phosphate-buffered saline (PBS), and rinsed in sterile water. The scaffolds were then disinfected in 70% ethanol for 24 h and dried in a sterile desiccator for 3 days. These scaffolds are hereafter referred to as *PCL scaffolds* (Fig. 1A).

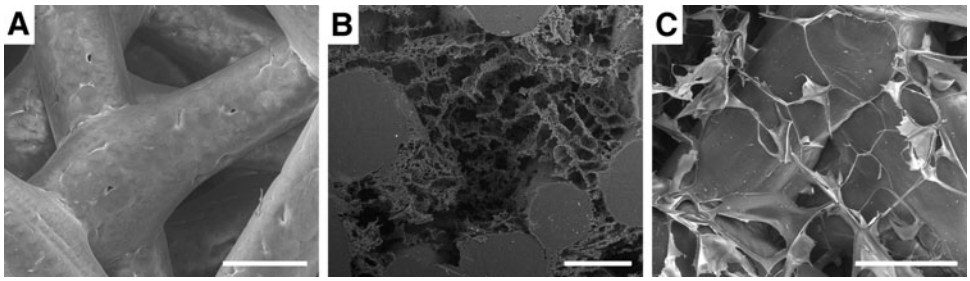

FIG. 1. Scanning electron microscopy of the polycaprolactone (PCL) fibers and embedded structure of the three different scaffold types. **(A)** Highly interconnected fiber structure of the purely fused deposition modeling (FDM)-manufactured PCL scaffold. **(B)** Nanostructured porous (NSP)-PCL scaffolds with the thermal induced phase separation (TIPS) PCL component embedded within the PCL fibers. The TIPS process resulted in various pore sizes with a high degree of interconnectivity and isotropic tubular morphology. **(C)** HT-PCL scaffold with thin hyaluronic acid (HA) coating creating an interconnected and highly porous network in between the PCL fibers. The β-TCP particles are dispersed on the surface of the PCL and HA. *White bars* = 200 μm.

One third of the PCL scaffolds were subsequently infused with a homogenous mixture of PCL (25 kDa), water, and 1,4-dioxane and underwent TIPS followed by lyophilization in a freeze dryer (FreeZone Triad Freeze Dry Systems, Labconco, Kansas City, MO) at −20°C for 4 days to introduce an interconnecting micro- and nano-porous structure within the PCL scaffold. The polymer concentration was 30 mg PCL/g 1,4-dioxane and the water concentration 0.0415 wt%. The procedure was optimized to achieve high interconnectivity, high porosity, and variable pore sizes when compared to previous constructs used.[10] This nanostructured porous (NSP) scaffold is for future reference called *NSP-PCL scaffold* (Fig. 1B).

The third scaffold type consisted of PCL scaffolds coated with HA and β-TCP manufactured using the following procedure: First, 4 mg/mL HA, 601 kDa −850 kDa (Lifecore Biomedical, Chaska, MN; Lot# 016066) was dissolved in distilled water and stored at 4°C for 24 h. Second, 6 mg β-TCP (Berkeley Advanced Biomaterials, Inc., Berkeley, CA; Lot# TCPCH01) per 15 mL HA solution was added and spun with a magnetic bar for approximately 10 min until uniform dispersion. Third, the PCL scaffolds were added to the HA-TCP solution and placed in a vacuum desiccator for 12 h. Finally, the scaffolds were placed in a freeze dryer (FreeZone Triad Freeze Dry Systems) at −20°C for 4 days. The final coated HA-TCP PCL scaffolds are referred to as *HT-PCL scaffolds* (Fig. 1C).

The scaffolds were qualitatively evaluated in relation to pore size and distribution using scanning electron microscopy (SEM) (Nova NanoSEM 600; FEI Company, Eindhoven, the Netherlands) and micro-computed tomography (μCT) (μCT 40; Scanco Medical AG, Zürich, Switzerland).

DPSC isolation and 3D culturing

Impacted fully developed healthy human third molars were surgically removed on the clinical indication of ectopia. Two donors were included: a 23-year-old male and a 20-year-old female.

The pulp was retrieved immediately after surgery and incubated for 30 min at 37°C in Dulbecco's minimum Essential medium (DMEM) (Gibco, 31966, Life Technologies Europe BV, Naerum, Denmark) containing 3 mg/mL of collagenase type I (Worthington Biochem, Freehold, NJ) and 2.4 units/mL of dispase II (Roche Diagnostics, Mannheim, Germany). DPSCs liberated from the pulp were passed through a 100-μm strainer (BD Biosciences–Discovery Labware, Bedford, MA). Cells were expanded in DMEM, supplemented with 10% fetal bovine serum (FBS) (Gibco, 10270, Life Technologies Europe BV) [hereafter referred to as *proliferation medium*] and antibiotics (25,000 IU/mL of penicillin and 25 mg/mL of streptomycin; DuraScan Medical Products, Odense, Denmark) at 37°C. Upon near confluence, DPSCs were harvested using 0.25% trypsin (Gibco, Life Technologies Europe BV) and 0.1% EDTA (Invitrogen, Taastrup, Denmark) in PBS. Cells were expanded by serial passaging and underwent three passages before seeding onto the scaffolds.

The protocol was approved by The Central Denmark Region Committee on Biomedical Research Ethics and conformed to Danish law.

Surface antigen analysis

DPSCs (passage 3) were trypsinized and resuspended in fluorescence-activated cell sorting (FACS) buffer (PBS with 1% BSA and 0,1% sodium azide) at a concentration of 2×10^6 cells per mL. A total of 2×10^5 cells were resuspended in a saturated solution of conjugated antibodies or an equivalent concentration of isotype-matched control IgG antibody in a final volume of 200 μL. The following allophycocyanin or fluorescein isothiocyanate (FITC)-conjugated murine anti-human antibodies was used at the manufacturer's recommended concentration (Abcam, Cambridge, United Kingdom): anti-CD14 FITC (ab28061), anti-CD90 FITC (ab124527), anti-CD105 allophycocyanin (ab155367), anti-CD73 allophycocyanin (ab155378), anti-IgG1 FITC isotype control (ab91356), and anti-IgG1 allophycocyanin isotype control (ab91358) (abcam). The samples were rinsed 3 times in FACS buffer subsequent to conjugation, resuspended in 500 μL cooled FACS buffer, and analyzed with flow cytometry on a Gallios™ Flow Cytometer (Beckman Coulter, Copenhagen, Denmark) using Kaluza Analysis Software (Beckman Coulter).

Three-dimensional cell culture

Scaffolds were placed in agarose-coated six-well plates with one scaffold per well. After 2 h incubation 100 μL cell suspension with 1×10^6 cells were applied drop-wise on top of the scaffolds. Cells were allowed to adhere for 2 h at 37°C in a humidified atmosphere of 5% CO_2 before proliferation media (7.5 mL/well) was added. After 7 days, medium was changed to osteogenic medium, which consisted of proliferation medium supplemented with 10 nM dexamethasone (D2915, Sigma-Aldrich, St. Louis, MO), 10 mM β-glycerophosphate (G9422; Sigma-Aldrich), and 283 μM L-ascorbic acid 2-phosphate (A8960; Sigma-Aldrich) [hereafter referred to as *osteogenic medium*]. The cells were cultured in osteogenic medium until day 21. Media were changed twice a week throughout the study.

All analyses were performed for all scaffold groups on day 1, 7, 14, and 21.

DNA quantification

Quantification of double-stranded DNA in each scaffold using the Quant-iT™ PicoGreen® dsDNA assay (Invitrogen) was used as a relative measure for cell numbers. Constructs were suspended in DMEM and sonicated at intervals of 1 s followed by 5 s pause for a total of 1 min to avoid heating during processing. Afterward, samples were prepared and analyzed according to protocol and as previously described using a Victor^3 1420 microspectrophotometer microplate reader (PerkinElmer Life Sciences, Waltham, MA).[12] Technical duplicates were used for each biological sample. Duplicate cell-free negative controls were analyzed for each scaffold type at each time point.

ALP activity

The ALP activity of the cells was determined by measuring the conversion of colorless p-nitrophenyl phosphate to yellowish p-nitrophenol on supernatant extracted following the sonication process during preparation for DNA quantification. To each 30 μL sample, 70 μL 2-amino-2-methyl-propanol buffer and 100 μL p-nitrophenyl phosphate (4 mg/mL) were added. Samples were incubated for 15 min at 37°C and the reaction was stopped by the addition of

100 μL 2 M NaOH. Absorbance of p-nitrophenol was measured at 405/650 nm using a Victor^3 microspectrophotometer microplate reader (Perkin Elmer Life Sciences). Technical duplicates were used for each biological sample. Duplicate cell-free negative controls were analyzed for each scaffold type at each time point.

Calcium contents assay

Calcium content in the 3D cultures was quantified by colorimetric endpoint assay utilizing the complexion of one calcium ion with two Arsenazo III (AZN) molecules to produce a detectable blue-purple product (Diagnostic Chemicals Limited, Charlottetown, PEI, Canada). The calcium deposition on scaffolds was dissolved in 1 M acetic acid for 7 days on a tilting table. The samples were diluted 1:50 with double-distilled water and aliquots of 20 μL were transferred to a 96-well plate. Arsenazo III solution (280 μL) was added and a standard dilution series of calcium ranging from 0 to 50 μg/mL was prepared. Ca^{2+}-concentration was quantified using the Victor^3 reader. Technical duplicates were used for each biological sample. Duplicate cell-free negative controls were analyzed for each scaffold type at each time point.

Real-time polymerase chain reaction

Total RNA from the scaffolds was extracted at all time points using the GenElute™ Mammalian Total RNA Miniprep Kit (RTN 350; Sigma-Aldrich) according to the manufacturer's instructions. RNA concentration and purity were spectrophotometrically determined using an IMPLEN Nano Photometer™ (VWR Bie & Berntsen, Herlev, Denmark) according to the manufacturer's instructions. RNA integrity was determined using an Agilent 2100 Bioanalyzer (Agilent Technologies, Santa Clara, CA) according to the procedure of the manufacturer. The RNA samples were treated with DNase I (AM2222; Ambion, Cambridgeshire, United Kingdom) and converted into complementary DNA (cDNA) using the High Capacity cDNA Reverse Transcription Kit (4368813; Applied Biosystems, Naerum, Denmark). Real-time quantitative polymerase chain reaction (RT-qPCR) was performed on a 7500 Fast Real-Time PCR system (Applied Biosystems) using TaqMan® Fast Universal PCR Master Mix (4366073; Applied Biosystems) and TaqMan Gene Expression Assays (4331182; Applied Biosystems) with following primers: bone morphogenetic protein 2 (*BMP-2*) Hs00154192_m1, collagen, type I, alpha 1 (*COL1A1*) Hs00164004_m1, alkaline phosphatase (*ALP*) Hs00758162_m1, bone gamma-carboxyglutamate (*GLA*) protein/osteocalcin (*OC*) Hs01587813_g1, bone sialoprotein I/osteopontin (*OPN*) Hs00167093_m1, and bone sialoprotein II (*BSP-II*) Hs00173720_m1 (all from Life Technologies Europe BV, Naerum, Denmark). Standard enzyme and cycling conditions for the 7500 Fast System were used. Template cDNA corresponding to 1 μg of RNA was added to each PCR reaction and each biological sample was run in technical duplicates for each gene. Data analysis was performed using 7500 Fast System Sequence Detection Software version 1.3 (Applied Biosystems).

Expression levels of the gene of interest were normalized to the BestKeeper index,[28] determined by the geometric mean of threshold cycles (Ct) from ubiquitin C (UBC) and RNA polymerase II (RPII).

Confocal and fluorescence imaging

To assess cell distribution and migration through the scaffold, cell/scaffold constructs from each time point were incubated for 30 min in DMEM containing 10 μM CellTracker™ Green CMFDA (5-Chloromethylfluorescein Diacetate; Invitrogen). The staining medium was then replaced with fresh DMEM/10% FBS and subsequently rinsed in PBS and fixed in 10% formalin. Surface images of the scaffolds were acquired using a laser scanning confocal microscope, 510 Meta (Zeiss Microimaging GmbH, Jena, Germany). Afterward, constructs were immersed in a PBS solution with 1 μg/mL Hoechst 33258 (Sigma-Aldrich). After 10 min, the constructs were rinsed in PBS and cut through the midline along the sagittal axis to reveal the entire center of the scaffold.

Scanning electron microscopy

Constructs were fixed in 2.5% glutaraldehyde containing 0.1 M sodium cacodylate buffer (pH 7.4) and dehydrated in a graded series of ethanol (50–99%) and subsequently transferred to an excicator for air-drying. Constructs were analyzed using a low vacuum secondary electron detector (Nova NanoSEM 600; FEI Company).

Statistics

Results followed a normal distribution when analyzed using D'Agostino's K^2 test. Results are presented graphically as mean ± standard deviation (SD) for $n = 4$ biological replicates. Results from each mean value were compared using two-way ANOVA with repeated measures (time*-scaffold type). Tukey's test was used to correct for multiple comparisons. A p-value of less than 0.05 was considered significant. STATA software (Ver. 12.1 StataCorp LP, College Station, TX) and PRISM (Ver. 6; GraphPad Software, Inc., San Diego, CA) were used for all calculations.

Results

DPSCs (passage 3) were subjected to surface antigen analysis for the expression of phenotypically relevant human MSCs markers ($CD90^+$, $CD73^+$, and $CD105^+$) and hematopoietic surface marker CD14. Our analysis of DPSCs surface marker expression by flow cytometry revealed that more than 95% of the total cell population expressed MSC markers $CD90^+$, $CD73^+$, and $CD105^+$, and less than 2% showed positivity for the hematopoietic markers CD14. FACS histograms are presented in Supplementary Data (Supplementary Fig. S1; Supplementary Data are available online at www.liebertpub.com/tea). These phenotypic results are in accordance with previous literature describing DPSCs.[29]

Cell seeding efficiency

The theoretical cell seeding efficiency can be calculated if assumed that no cellular division happens during the first 24 h and the DNA assay utilized possess 100% detectability. The scaffolds were all seeded with 1×10^6 cells. Assuming the DNA yield from 1×10^6 cells $\approx$ 6.9 μg DNA, the seeding efficiency on PCL, NSP-PCL, and HT-PCL scaffolds were 41% ± 2%, 36% ± 3%, and 35% ± 3% respectively. No

statistically significant difference in seeding efficiency was observed.

Cellular distribution and viability

The surface of the top of the scaffolds was visualized with confocal microscopy (Fig. 2A–C). A homogenous cell distribution was observed earlier on the surface of the NSP-PCL scaffold compared to the other two scaffold types. On day 21, cells were evenly dispersed on the surface of all three scaffold types (Fig. 2A–C).

SEM images were used to evaluate cell morphology and adhesion to the scaffold surface. On day 21, cells tended to cluster around fiber junctions in the PCL scaffolds, where cells stretched out to attach with focal adhesion points on the adjacent fibers (Fig. 2D). Cells on the NSP-PCL scaffolds were generally more evenly dispersed on the surface of the scaffold adhesion points, and they were in general more abundant compared with the PCL scaffolds (Fig. 2E). Less clustering of cells was also observed in the HT-PCL scaffold and most cells appeared to be attached to the PCL fibers (Fig. 2F).

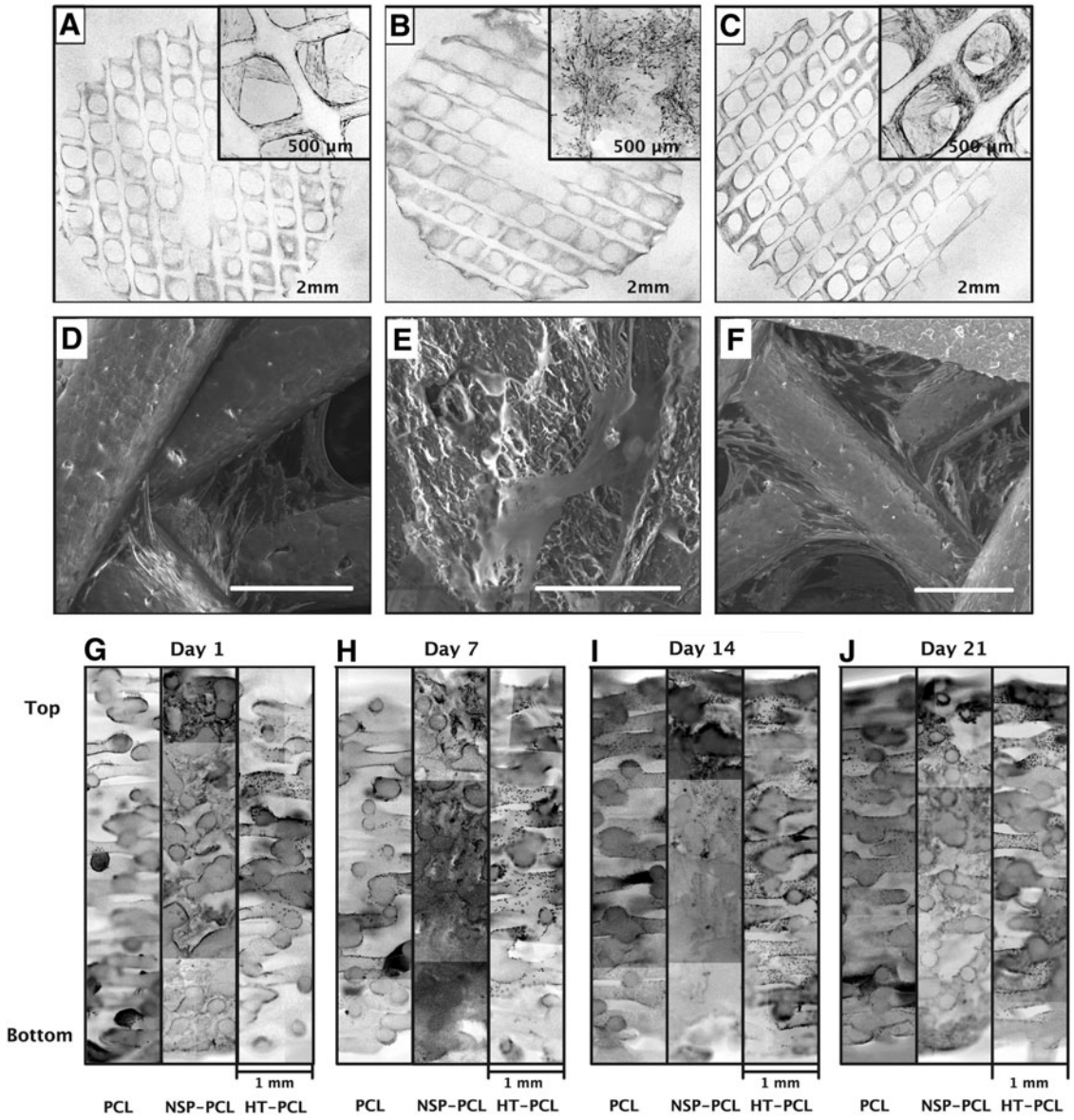

FIG. 2. **(A–C)** Confocal micrographs of whole scaffold surface (cell seeding side) after CellTracker™ *Green* staining. Original magnification x4 of representative areas of interest superimposed in the *upper right* corner. **(D–F)** SEM images representing cell adhesion characteristics on the scaffold surface. *White bar* represents 200 µm. **(A, D)** PCL scaffold, **(B, E)** NSP-PCL scaffold, and **(C, F)** HT-PCL scaffold. All images from **(A–F)** are acquired from scaffolds from day 21. **(G–J)** Hoechst staining of cell nuclei on histology sections from each scaffold on day 1**(G)**, 7**(H)**, 14**(I)**, and 21**(J)**. Each picture represents a section through the entire height of the scaffold. Image was color inverted and transformed from *black* background with *blue* fluorescence, to *white* background with grayscale fluorescence. An unedited color image of the fluoroscopy is available as Supplementary Data (Supplementary Fig. S2).

Cellular distribution throughout the scaffolds was visualized by fluorescent staining (Hoechst) (Fig. 2G–J). The evaluation on day 1 is presumed to visualize the initial cell distribution within the scaffold after seeding of cells. In the PCL scaffolds, cells clustered into small groups toward the bottom of the scaffold. In the top, a more dispersed cell distribution on the PCL fibers was observed. On the NSP-PCL scaffolds cell penetration was limited to the top 1 mm, where a high concentration of cells was observed. The cells were more evenly dispersed in the HT-PCL scaffold, but mainly located in the top half of the scaffold. On day 7 and 14, cells became more dispersed in the PCL scaffold, but cells still formed large clusters throughout the scaffold. In the NSP-PCL scaffold cells started to migrate down through the construct, reaching a depth of 3 mm on day 14. In the HT-PCL scaffold cells increased in number and became evenly dispersed throughout the scaffold. On day 21, cells in the PCL scaffold were distributed throughout the entire scaffold. However, cells still had a tendency to cluster, especially toward the bottom of the scaffold. In the NSP-scaffolds, cells were visible throughout the scaffold, but a gradient toward fewer cells in the bottom of the scaffold was evident. In the HT-PCL scaffolds, an increase in cell density and even distribution was observed.

DNA quantification

The DNA amount was assumed proportional to the cell number. Thus, cell proliferation over time could be monitored by DNA extraction from the scaffolds (Fig. 3). No increase in cell number was observed for all three scaffold types during the first 7 days. From day 7 to 14, both the PCL and HT-PCL groups saw a significant increase in quantified DNA. In this time period, DNA extracted from the NSP-PCL scaffold decreased significantly. A significant increase in DNA from day 14 to 21 was observed on all three scaffold types. On day 21, the DNA yield was highest for the HT-PCL scaffolds and lowest for NSP-PCL scaffolds, while the DNA yield of the PCL scaffolds lay in between. All of these differences reached highly statistical significance. Cell-free controls did not exhibit any assay activity.

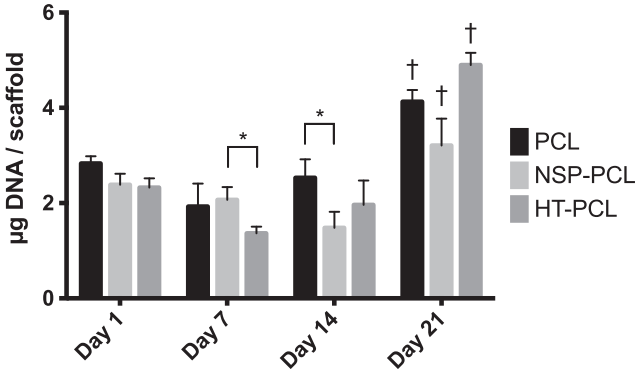

FIG. 3. DNA quantification as a surrogate for cell number on day 1, 7, 14, and 21. The amount of DNA is expressed as mean ± SD ($n = 4$). *Indicates a significant difference between two groups bracketed at the same time point ($p < 0.05$). †Indicates significant difference between the marked group and the two other groups at the same time point ($p < 0.05$).

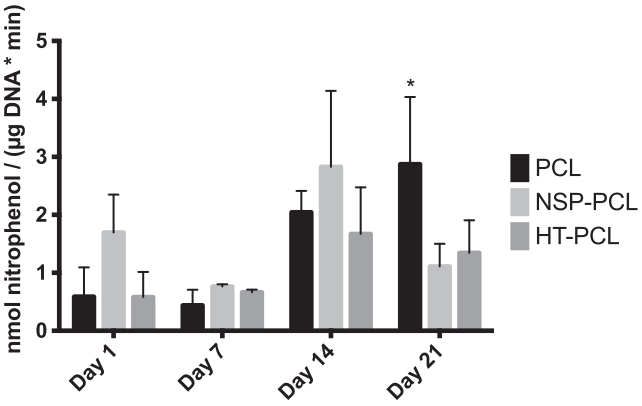

FIG. 4. Alkaline phosphatase (ALP) activity on day 1, 7, 14, and 21. The activity is expressed as mean ± SD ($n = 4$). *Significant difference between the marked group and the two other groups at the same time point ($p < 0.05$).

ALP activity

The ALP activity was analyzed with regard to the cell number (Fig. 4). No significant difference in ALP activity was present between day 1 and 7 or within scaffold types. From day 7 to 14, ALP activity significantly increased in all three groups but no significant difference within the three scaffold types was observed. The ALP activity in the PCL scaffolds was significantly higher than both other groups at day 21. Cell-free controls did not exhibit any assay activity.

Mineralization

The Ca^{2+} content in the scaffolds is depicted in Figure 5. No cell-mediated Ca^{2+} deposition was present on any scaffold until day 14. The HT-PCL group exhibited significantly higher Ca^{2+} content on day 14 compared with both

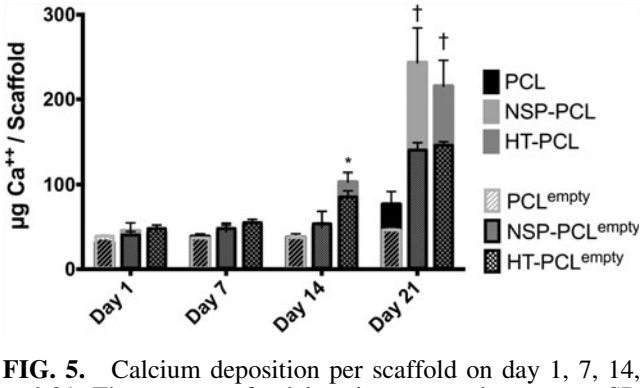

FIG. 5. Calcium deposition per scaffold on day 1, 7, 14, and 21. The amount of calcium is expressed as mean ± SD ($n = 4$). *Significant difference between the marked group and the two other groups at the same time point ($p < 0.05$). †Significant higher calcium deposition than the PCL scaffold group at the same time point ($p < 0.05$). Detection values from negative empty scaffold controls ($n = 2$) are superimposed on the graph and labeled x^{empty}.

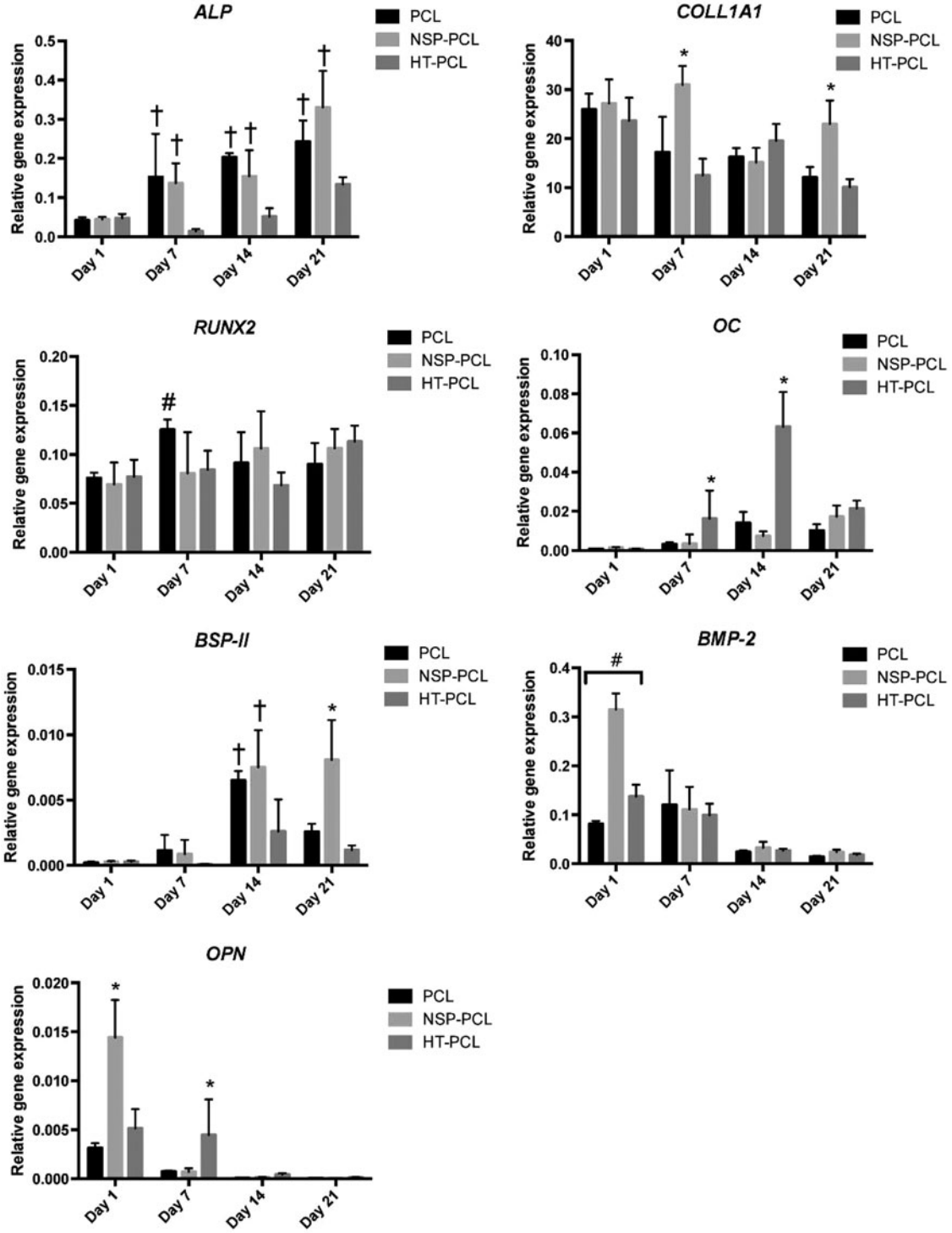

FIG. 6. Real-time quantitative polymerase chain reaction results of osteogenic markers after 1, 7, 14, and 21 days. The results are expressed as mean ± SD ($n = 4$). #Significant difference between all the groups bracketed at the same time point ($p < 0.05$). *Significant difference between the marked group and the two other groups at the same time point ($p < 0.05$). †Significant difference between the marked group and the HT-PCL group at the same time point ($p < 0.05$). #Significantly higher *RUNX2* gene expression in the PCL group compared with day 1 ($p < 0.05$).

other groups. An increase in Ca^{2+} deposition from day 14 to 21 was observed in both the NSP-PCL and HT-PCL group. No significant difference was found between these two groups on day 21. The Ca^{2+} assay displayed a substantial AZN deposition on the NSP-PCL and HT-PCL scaffold on day 21, which converted to high values in the negative controls. Negative controls were not subtracted from the intervention groups prior to statistical evaluation. The negative controls are instead superimposed on the intervention group values in Figure 5.

Quantitative RT-PCR

The gene expression of osteogenic markers *ALP*, *COLL1A1*, *RUNX2*, *OC*, *BSP-II*, *BMP-2*, and *OPN* were determined using RT-qPCR (Fig. 6). *ALP* gene expression in both the PCL and NSP-PCL scaffolds displayed significantly higher gene expressions than the HT-PCL scaffold on both day 7, 14, and 21. A delayed *ALP* gene expression was observed for the HT-PCL scaffold. *COLL1A1* levels displayed a slow decline from day 1 and throughout the study in both the PCL and HT-PCL groups. The NSP-PCL group showed a significant peak in gene expression on day 7 and 21. *RUNX2* gene expression exhibited an almost constant rate throughout the study except for a significant increase in expression observed in PCL scaffolds from day 1 to 7. No significant differences were observed between scaffold groups at any time point. On day 7, significantly higher *OC* levels were detected in the HT-PCL scaffold group, which was further emphasized on day 14. *BSP-II* expression exhibited, opposite to *OC*, significantly higher levels in both the PCL and NSP-PCL group on day 14. On day 21, *BSP-II* expression was significantly higher in the NSP-PCL scaffold group than in the two other groups.

BMP-2 gene expression exhibited highest activity on day 1, especially on the NSP-PCL scaffold. Significant differences were observed between all three scaffold types with relative gene expression levels: NSP-PCL > HT-PCL > PCL. The gene expression equalized between the three scaffold types on day 7 and dropped afterward to almost no expression at day 14 and 21. *OPN* gene expression showed a similar trend for day 1 although only NSP-PCL scaffolds exhibited significantly higher values than the other two groups. On day 7, *OPN* activity was only present in the HT-PCL scaffolds. No *OPN* activity was observed on day 14 and 21 in either group.

Discussion

This study evaluated the osteogenic differentiation and cellular distribution of DPSCs in three different scaffolds based on the same PCL backbone. The three different approaches toward functionalization provided a novel insight into the response of DPSCs on the different scaffold modalities. Two key observations were made in this study. The first one was the DPSCs' ability to migrate into the PCL and HT-PCL constructs and homogenously distribute throughout the scaffolds. The second one was the proliferation and subsequent differentiation of DPSCs into bone forming cells, resulting in Ca^{2+} deposition, most notably in the NSP-PCL and HT-PCL scaffolds.

By analyzing the scaffolds using fluorescence microscopy, we qualitatively observed a larger cell penetration and more even dispersion in the HT-PCL scaffolds earlier and more pronounced on day 21. The structural porosity and the hydrophilic nature of the HA were likely causes for this early observation, and it was facilitated further by the stimulation of cell motility by the HA. Similar to previous studies, the TIPS-manufactured compound embedded between the fibers of the NSP-PCL scaffold impaired the cell penetration into the scaffold.[30,31] The hydrophobic properties of PCL together with a large proportion of pores with a diameter less than 100 μm was most likely the primary cause. Cells were primarily concentrated in clusters or in the bottom of the PCL scaffolds on day 1 followed by a slow dispersion. This phenomenon suggests that the pore structure was too open to allow trapping of cells when seeding drop-wise. Furthermore, cells probably tended to cluster due to the low surface area and hydrophobic surface.

The PCL group did, however, exhibit seeding efficiency similar to both the HT-PCL and NSP-PCL group. This could be due to the drop-wise seeding technique resulting in cell spill on the denser HT-PCL and NSP-PCL scaffolds. Another reason could be the large height of the scaffolds enabling a proportionately higher amount of cells to be trapped within the PCL scaffold since this scaffold, due to the open pore structure, causes a large proportion of the cells to be trapped toward the bottom of the scaffold.

The size and structural composition of the scaffolds did, however, not appear to inflict on the cell seeding efficiency, which exhibited a comparable or even higher efficiency than other similar scaffolds.[32–34]

ALP is an enzyme produced by active osteoblasts involved in the early induction of mineralization of newly formed bone tissue. A significant increase in ALP activity was observed from day 7 to 14 in all three scaffold types. The ALP activity continued to rise in the PCL group, resulting in a significantly higher activity than the two other groups on day 21. A possible reason for this observation could be that the ALP activity within the NSP-PCL and HT-PCL groups peaked between day 14 and 21. If true, this would explain the significantly higher Ca^{2+} deposition in the NSP-PCL and HT-PCL groups on day 21 while an increase could be observed at a later time point in the PCL group. The late onset increase in ALP activity could be due to the initial 7 days of culture in proliferation media, which was intended as a stimulation of cell migration prior to osteogenic differentiation. However, an increase in ALP gene expression was observed in the PCL and NSP-PCL groups on day 7 suggesting that DPSCs are less dependent on medium stimulation to initiate osteogenic differentiation. Another reason could be that the scaffold morphology promotes osteogenic differentiation in itself by cell-surface contact stimulation, which was consistent with our observation that there were more condensed cell distribution on the surface of the PCL and NSP-PCL scaffolds on day 1.

BMP-2 gene expression, which indicates early initiation of osteoblastic differentiation, showed most activity on day 1 and 7.[35] Most notable was the high expression by cells cultured on the NSP-PCL scaffold on day 1 suggesting an early commencement of osteogenic differentiation, which is supported by the presented ALP results. This early initiation of differentiation does not result in increased Ca^{2+} deposition, which might be caused by the lack of components in the proliferation medium to ascertain and sustain this early osteogenic response. *OPN* expression also peaked early as expected since *OPN* expression indicates the degree of motility elicited by the cells.[36] The NSP-PCL group had the highest *OPN* expression level, which could potentially be explained by the higher demand for cell migration stimulation due to the denser pore structure of the scaffold compared with the two other scaffold types, in which large pore size enabled easier dispersion through the scaffold without the need for stimulation. The HT-PCL group exhibited significantly higher *OPN* values on day 7 compared with the two other groups. A possible explanation of this

finding could be the combination of 7 days in proliferation medium and the presence on HA in the scaffold. HA is a very large glycosaminoglycan present in abundance in the ECM. The size and hydrophilicity of the molecule are important functional properties adding turgor and mechanical resilience to tissues, especially those in the musculoskeletal system. In the ECM, HA contributes to tissue hydrodynamics, modulation of cell attachment strength, motility, and proliferation. It participates in a number of cell surface receptor interactions, most notably through its primary receptors, CD44 and CD168.[37] Pathways that determine cell morphology and survival can also be triggered by CD44 receptor–ligand interactions. HA has previously been demonstrated to bind specifically and with high affinity to intact cells, and to enhance cell motility on two-dimensional culture surfaces.[38] One of the methods by which HA stimulates cell motility is by regulating Ras signaling through the receptor for hyaluronan-mediated motility (RHAMM, CD168).[39] The ability of HA to increase cell motility in scaffolds has been shown previously,[12] and could be the primary reason for a sustained *OPN* gene expression thorough day 7 and the early even dispersion of cells through the scaffold found with fluoroscopy.

MSCs differentiate into immature osteoblasts that express bone matrix protein genes downstream of RUNX2 (e.g., *OC*, *BSP-II*, and *COLL1A1*). The *RUNX2* gene expression displayed an almost constant level unaffected by scaffold type and time point. The reason for this could be that the *RUNX2* expression peaked between two observation times, probably day 7 and 14, and therefore not detected by our assays.

The expression of transcription factor *RUNX2* resulted in a significant upregulation in *OC* gene expression in the HT-PCL group on day 14. Osteocalcin is produced by mature osteoblasts, promotes mineralization and formation of bone, and is the most abundant noncollagenous protein in the matrix (10–20% of total).[40] The OC upregulation in the HT-PCL group corresponds well to the rapid increase in Ca^{2+} deposition observed on day 21. *BSP-II* was significantly higher expressed in the PCL and NSP-PCL group on day 14 and in the NSP-PCL group on day 21. *BSP-II* is a mineralized tissue-specific protein that is expressed in differentiated osteoblasts and appears to function in the initial formation of apatite crystals and mineralization of bone.[41,42]

However, only the NSP-PCL group and not the PCL group exhibited significant increase in Ca^{2+} deposition on day 21. The divergence between the two genes that upregulates depending on scaffold type suggests that the morphological structure of the scaffold plays distinctive roles in the differentiation to osteoblasts and subsequent osteogenic response.

The negative controls cultured under same settings as the scaffolds with cells, only expressed small amounts in the ALP and DNA assays. The AZR staining, which was implemented to quantify Ca^{2+} deposition on the scaffolds did, however, express notably high values–especially in the NSP-PCL and HT-PCL groups after 21 days. We therefore chose to superimpose all the cell-free control values on the Ca^{2+} graph. We suspect that both scaffold types trapped/deposited the Ca^{2+} ions from the culture medium, which caused an inadvertently high AZR conversion and subsequent detection. In the case of the HT-PCL scaffold, negative charge of HA could bind the positive charge of Ca^{2+} ions.[43] As with the Ca^{2+} content from the medium, we believe that the HA component in the scaffold bound the β-TCP within the surface coating and thereby inhibited a Ca^{2+} release from the scaffold until day 14. We chose not to subtract the data from the cell-free controls since comparison of a cell-coated scaffold with a cell-free scaffold would insinuate that cells covering the surface did not inflict on the potential Ca^{2+} deposition from surrounding medium. Taking the results from the cell-free controls into account does not inflict on the conclusion that more Ca^{2+} were deposited on the cell-loaded NSP-PCL and HT-PCL scaffolds compared to the PCL scaffolds. The trapping of Ca^{2+} ions from surrounding medium could potentially prove beneficiary due to higher Ca^{2+} bioavailability for bone forming cells at the defect site *in vivo*.

Previous *in vitro* investigations of the osteogenesis of DPSCs have primarily been conducted on smaller scaffolds.[44–48] The discrepancy in size between scaffolds tested *in vitro* and scaffolds applied in bone defects are often large, so we sought to assess the osteogenic potential on large, clinically relevant scaffolds. Parallels between static *in vitro* culturing and an *in vivo* environment in terms of nutrient flow and micro environmental conditions are limited. Culturing in a dynamic culturing environment like spinner flasks could therefore have been advantageous but holds the risk of overestimating the performance of large scaffolds. However, if a sufficient milieu for cell migration and viability throughout the scaffold were present during static culturing, the same would be presumed true for the dynamic environment *in vivo*.

Comparing DPSCs to BMSCs has so far only been conducted on gene level and as a facilitator of implant fixation *in vivo*.[49,50] Since this study is limited by assessing the osteogenic potential of DPSCs only, a future study comparing the two cell types to quantify the potential osteogenic difference *in vitro* could be of interest.

In conclusion, DPSCs displayed the ability to differentiate into an osteogenic lineage capable of facilitating Ca^{2+} deposition on the scaffolds. Both the NSP-PCL and HT-PCL scaffold promoted Ca^{2+} deposition after 21 days of cultivation on large scaffolds, which was significantly higher than on the PCL scaffold. This observation was supported by a tendency toward earlier differentiation facilitated on the functionalized NSP-PCL and HT-PCL scaffolds compared with the PCL scaffold. However, only the HT-PCL scaffold exhibited these properties while supporting cell proliferation and cell migration resulting in even dispersion throughout the scaffold. The ability to stimulate cells to undergo osteogenic differentiation while promoting cell migration throughout a large scaffold in static culture, makes the HA and β-TCP functionalized PCL scaffold a promising scaffold for use in large bone defect repair.

Acknowledgments

The authors would like to thank lab technicians Anette Baatup, Lisbeth Ann Abildtrup, and Jane Pauli for expert assistance.

The study received funding from the Individualized Musculoskeletal Regeneration and Reconstruction Network, Ministry of Science, Innovation and Higher Education, Denmark; contract grant number: 8415 and The Lundbeck

Foundation Nanomedicine Centre for Individualized Management of Tissue Damage and Regeneration (LUNA).

Disclosure Statement

A spin-off company (Levoss Aps, Copenhagen, Denmark) has later been established based on a patent filed on the NSP-PCL scaffold.[51] The author Cody Eric Bünger is financially involved with this company, however, the company has contributed neither financially nor in any other way to this study.

All other authors declare that no competing financial interests exist.

References

1. Dimitriou, R., Jones, E., McGonagle, D., and Giannoudis, P.V. Bone regeneration: current concepts and future directions. BMC Med **9,** 66, 2011.
2. Schroeder, J.E., and Mosheiff, R. Tissue engineering approaches for bone repair: concepts and evidence. Injury **42,** 609, 2011.
3. Lutolf, M.P., and Hubbell, J.A. Synthetic biomaterials as instructive extracellular microenvironments for morphogenesis in tissue engineering. Nat Biotechnol **23,** 47, 2005.
4. Lichte, P., Pape, H.C., Pufe, T., Kobbe, P., and Fischer, H. Scaffolds for bone healing: concepts, materials and evidence. Injury **42,** 569, 2011.
5. Bruinink, A., Bitar, M., Pleskova, M., Wick, P., Krug, H.F., and Maniura-Weber, K. Addition of nanoscaled bioinspired surface features: A revolution for bone-related implants and scaffolds? J Biomed Mater Res A **102,** 275, 2013.
6. Hutmacher, D.W., Schantz, T., Zein, I., Ng, K.W., Teoh, S.H., and Tan, K.C. Mechanical properties and cell cultural response of polycaprolactone scaffolds designed and fabricated via fused deposition modeling. J Biomed Mater Res **55,** 203, 2001.
7. Hutmacher, D.W., Schantz, J.T., Lam, C.X.F., Tan, K.C., and Lim, T.C. State of the art and future directions of scaffold-based bone engineering from a biomaterials perspective. J Tissue Eng Regen Med **1,** 245, 2007.
8. Derby, B. Printing and prototyping of tissues and scaffolds. Science **338,** 921, 2012.
9. Christensen, B.B., Foldager, C.B., Hansen, O.M., Kristiansen, A.A., Le, D.Q.S., Nielsen, A.D., *et al.* A novel nano-structured porous polycaprolactone scaffold improves hyaline cartilage repair in a rabbit model compared to a collagen type I/III scaffold: *in vitro* and *in vivo* studies. Knee Surg Sports Traumatol Arthrosc **20,** 1192, 2012.
10. Jensen, J., Rölfing, J.H.D., Svend Le, D.Q., Kristiansen, A.A., Nygaard, J.V., Hokland, L.B., *et al.* Surface-modified functionalized polycaprolactone scaffolds for bone repair: *In vitro* and *in vivo* experiments. J Biomed Mater Res A **102,** 2993, 2014.
11. Zou, L., Zou, X., Chen, L., Li, H., Mygind, T., Kassem, M., *et al.* Effect of hyaluronan on osteogenic differentiation of porcine bone marrow stromal cells *in vitro*. J Orthop Res **26,** 713, 2008.
12. Chen, M., Le, D.Q.S., Baatrup, A., Nygaard, J.V., Hein, S., Bjerre, L., *et al.* Self-assembled composite matrix in a hierarchical 3-D scaffold for bone tissue engineering. Acta Biomater **7,** 2244, 2011.
13. Zou, L., Luo, Y., Chen, M., Wang, G., Ding, M., Petersen, C.C., *et al.* A simple method for deriving functional MSCs and applied for osteogenesis in 3D scaffolds. Sci Rep **3,** 2243, 2013.
14. Caplan, A.I. Adult mesenchymal stem cells for tissue engineering versus regenerative medicine. J Cell Physiol **213,** 341, 2007.
15. Caplan, A.I., and Dennis, J.E. Mesenchymal stem cells as trophic mediators. J Cell Biochem **98,** 1076, 2006.
16. Simonsen, J.L., Rosada, C., Serakinci, N., Justesen, J., Stenderup, K., Rattan, S.I.S., *et al.* Telomerase expression extends the proliferative life-span and maintains the osteogenic potential of human bone marrow stromal cells. Nat Biotechnol **20,** 592, 2002.
17. Chamberlain, G., Fox, J., Ashton, B., and Middleton, J. Concise review: mesenchymal stem cells: their phenotype, differentiation capacity, immunological features, and potential for homing. Stem Cells **25,** 2739, 2007.
18. Graziano, A., d'Aquino, R., Laino, G., and Papaccio, G. Dental pulp stem cells: a promising tool for bone regeneration. Stem Cell Rev **4,** 21, 2008.
19. Kraft, D.C.E., Bindslev, D.A., Melsen, B., and Klein-Nulend, J. Human dental pulp cells exhibit bone cell-like responsiveness to fluid shear stress. Cytotherapy **13,** 214, 2011.
20. Perry, B.C., Zhou, D., Wu, X., Yang, F.-C., Byers, M.A., Chu, T.-M.G., *et al.* Collection, cryopreservation, and characterization of human dental pulp-derived mesenchymal stem cells for banking and clinical use. Tissue Eng Part C Methods **14,** 149, 2008.
21. Goldberg, M., and Smith, A.J. Cells and extracellular matrices of dentin and pulp: a biological basis for repair and tissue engineering. Crit Rev Oral Biol Med **15,** 13, 2004.
22. Gronthos, S., Brahim, J., Li, W., Fisher, L.W., Cherman, N., Boyde, A., *et al.* Stem cell properties of human dental pulp stem cells. J Dent Res **81,** 531, 2002.
23. Laino, G., d'Aquino, R., Graziano, A., Lanza, V., Carinci, F., Naro, F., *et al.* A new population of human adult dental pulp stem cells: a useful source of living autologous fibrous bone tissue (LAB). J Bone Miner Res **20,** 1394, 2005.
24. d'Aquino, R., Graziano, A., Sampaolesi, M., Laino, G., Pirozzi, G., De Rosa, A., *et al.* Human postnatal dental pulp cells co-differentiate into osteoblasts and endotheliocytes: a pivotal synergy leading to adult bone tissue formation. Cell Death Differ **14,** 1162, 2007.
25. Kraft, D.C.E., Bindslev, D.A., Melsen, B., Abdallah, B.M., Kassem, M., and Klein-Nulend, J. Mechanosensitivity of dental pulp stem cells is related to their osteogenic maturity. Eur J Oral Sci **118,** 29, 2010.
26. Mangano, C., De Rosa, A., Desiderio, V., d'Aquino, R., Piattelli, A., De Francesco, F., *et al.* The osteoblastic differentiation of dental pulp stem cells and bone formation on different titanium surface textures. Biomaterials **31,** 3543, 2010.
27. Akkouch, A., Zhang, Z., and Rouabhia, M. Engineering bone tissue using human dental pulp stem cells and an osteogenic collagen-hydroxyapatite-poly (L-lactide-co-ε-caprolactone) scaffold. J Biomater Appl **28,** 922, 2014.
28. Pfaffl, M.W., Tichopad, A., Prgomet, C., and Neuvians, T.P. Determination of stable housekeeping genes, differentially regulated target genes and sample integrity: BestKeeper–Excel-based tool using pair-wise correlations. Biotechnol Lett **26,** 509, 2004.
29. Huang, G.T.J., Gronthos, S., and Shi, S. Mesenchymal stem cells derived from dental tissues vs. those from other sources: their biology and role in regenerative medicine. J Dent Res **88,** 792, 2009.

30. Ishaug-Riley, S.L., Crane-Kruger, G.M., Yaszemski, M.J., and Mikos, A.G. Three-dimensional culture of rat calvarial osteoblasts in porous biodegradable polymers. Biomaterials **19,** 1405, 1998.
31. Zhang, Z.-Y., Teoh, S.H., Chong, W.-S., Foo, T.-T., Chng, Y.-C., Choolani, M., *et al.* A biaxial rotating bioreactor for the culture of fetal mesenchymal stem cells for bone tissue engineering. Biomaterials **30,** 2694, 2009.
32. Papadimitropoulos, A., Riboldi, S.A., Tonnarelli, B., Piccinini, E., Woodruff, M.A., Hutmacher, D.W., *et al.* A collagen network phase improves cell seeding of open-pore structure scaffolds under perfusion. J Tissue Eng Regen Med **7,** 183, 2013.
33. Bjerre, L., Bünger, C., Baatrup, A., Kassem, M., and Mygind, T. Flow perfusion culture of human mesenchymal stem cells on coralline hydroxyapatite scaffolds with various pore sizes. J Biomed Mater Res A **97A,** 251, 2011.
34. Zhang, W., Walboomers, X.F., van Osch, G.J.V.M., van den Dolder, J., and Jansen, J.A. Hard tissue formation in a porous HA/TCP ceramic scaffold loaded with stromal cells derived from dental pulp and bone marrow. Tissue Eng Part A **14,** 285, 2008.
35. Chatakun, P., Núñez-Toldrà, R., Díaz López, E.J., Gil-Recio, C., Martínez-Sarrà, E., Hernández-Alfaro, F., *et al.* The effect of five proteins on stem cells used for osteoblast differentiation and proliferation: a current review of the literature. Cell Mol Life Sci **71,** 113, 2014.
36. Suzuki, K., Zhu, B., Rittling, S.R., Denhardt, D.T., Goldberg, H.A., McCulloch, C.A.G., *et al.* Colocalization of intracellular osteopontin with CD44 is associated with migration, cell fusion, and resorption in osteoclasts. J Bone Miner Res **17,** 1486, 2002.
37. Aruffo, A., Stamenkovic, I., Melnick, M., Underhill, C.B., and Seed, B. CD44 is the principal cell surface receptor for hyaluronate. Cell **61,** 1303, 1990.
38. Underhill, C.B., and Toole, B.P. Binding of hyaluronate to the surface of cultured cells. J Cell Biol **82,** 475, 1979.
39. Turley, E.A., Noble, P.W., and Bourguignon, L.Y.W. Signaling properties of hyaluronan receptors. J Biol Chem **277,** 4589, 2002.
40. Komori, T. Regulation of osteoblast differentiation by transcription factors. J Cell Biochem **99,** 1233, 2006.
41. Hunter, G.K., and Goldberg, H.A. Modulation of crystal formation by bone phosphoproteins: role of glutamic acid-rich sequences in the nucleation of hydroxyapatite by bone sialoprotein. Biochem J **302 (Pt 1),** 175, 1994.
42. Wang, S., Sasaki, Y., Zhou, L., Matsumura, H., Araki, S., Mezawa, M., *et al.* Transcriptional regulation of bone sialoprotein gene by interleukin-11. Gene **476,** 46, 2011.
43. Hunter, G.K., Wong, K.S., and Kim, J.J. Binding of calcium to glycosaminoglycans: an equilibrium dialysis study. Arch Biochem Biophys **260,** 161, 1988.
44. Lee, C.H., Hajibandeh, J., Suzuki, T., Fan, A., Shang, P., and Mao, J.J. Three-dimensional printed multiphase scaffolds for regeneration of periodontium complex. Tissue Eng Part A **20,** 1342, 2014.
45. Yang, X., Han, G., Pang, X., and Fan, M. Chitosan/collagen scaffold containing bone morphogenetic protein-7 DNA supports dental pulp stem cell differentiation *in vitro* and *in vivo*. J Biomed Mater Res A 2012 [Epub ahead of print]; DOI: 10.1002/jbm.a.34064.
46. Zheng, L., Yang, F., Shen, H., Hu, X., Mochizuki, C., Sato, M., *et al.* The effect of composition of calcium phosphate composite scaffolds on the formation of tooth tissue from human dental pulp stem cells. Biomaterials **32,** 7053, 2011.
47. Wang, J., Liu, X., Jin, X., Ma, H., Hu, J., Ni, L., *et al.* The odontogenic differentiation of human dental pulp stem cells on nanofibrous poly(L-lactic acid) scaffolds *in vitro* and *in vivo*. Acta Biomater **6,** 3856, 2010.
48. Yang, X., Yang, F., Walboomers, X.F., Bian, Z., Fan, M., and Jansen, J.A. The performance of dental pulp stem cells on nanofibrous PCL/gelatin/nHA scaffolds. J Biomed Mater Res A **93,** 247, 2010.
49. Yamada, Y., Fujimoto, A., Ito, A., Yoshimi, R., and Ueda, M. Cluster analysis and gene expression profiles: a cDNA microarray system-based comparison between human dental pulp stem cells (hDPSCs) and human mesenchymal stem cells (hMSCs) for tissue engineering cell therapy. Biomaterials **27,** 3766, 2006.
50. Ito, K., Yamada, Y., Nakamura, S., and Ueda, M. Osteogenic potential of effective bone engineering using dental pulp stem cells, bone marrow stem cells, and periosteal cells for osseointegration of dental implants. Int J Oral Maxillofac Implants **26,** 947, 2011.
51. Bjerre, L., Nygaard, J.V., and Bünger, C.E. Three-dimensional nanostructured hybrid scaffold and manufacture thereof. EP Patent UA20120128739, 2010.

Address correspondence to:
Jonas Jensen, MD
Orthopaedic Research Laboratory
Aarhus University Hospital
Noerrebrogade 44, Building 1A
Aarhus 8000
Denmark

E-mail: jj@clin.au.dk

Received: March 25, 2014
Accepted: September 15, 2014
Online Publication Date: October 30, 2014